20th Optics of Liquid Crystals Conference (OLC2023), Szczecin, Poland

Opto-Electronics Review 32 (2024) e151693

Opto-Electronics Review

journal homepage: https://journals.pan.pl/opelre

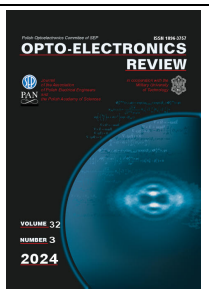

Induced blue phase and twist grain boundary phase in binary mixtures of chiral calamitic and achiral hockey stick-shaped liquid crystals

Smriti Mitra[1], Priyanta Barman[1], Malay K. Das[1*], Věra Hamplová[2], Alexej Bubnov[2]

[1] Department of Physics, University of North Bengal, Siliguri-734013, West Bengal, India
[2] Institute of Physics, Czech Academy of Science, 18200, Prague, Czech Republic

Article info

Article history:
Received 10 Nov. 2023
Received in revised form 14 Jun. 2024
Accepted 14 Jul. 2024
Available on-line 22 Sep. 2024

Keywords:
Ferroelectric liquid crystals;
hockey stick-shaped compound;
lactic acid derivative;
blue phase;
TGB_A^* phase.

Abstract

Frustrated phases in chiral liquid crystalline systems, such as the blue phase (BP) and the twist grain boundary (TGB) phase, can create new opportunities in liquid crystal research. These frustrated phases have unique optical properties which can be used for specific applications. A new binary mixture system composed of a chiral rod-like ferroelectric liquid crystal and an achiral hockey stick-shaped compound was designed. This binary system exhibits induced frustration, resulting in the emergence of the BP-III and TGB_A^* phases in addition to the chiral ferroelectric Smectic-C^* phase. We report a comprehensive study on several binary mixtures ($x_{H\text{-}22.5} = 0.162, 0.25, 0.396, 0.562$) designed of a chiral ferroelectric liquid crystal derived from the lactic acid, namely 4-(octyloxy)phenyl 3-methoxy-4-((4-((2-(pentyloxy)propanoyl)oxy)benzoyl)oxybenzoate and achiral hockey stick-shaped compound, namely (E)-4-((E-((3-(decyloxy)-2-methylphenyl)imino)methyl)-phenyl 3-(4-(dodecyloxy)phenyl)acrylate. These mixtures induced the blue phase (BP-III, ~2.5–6.2K) and the twist grain boundary Smectic-A^*phase (TGB_A^* ~1.8–6K). Polarizing optical microscopy, birefringence, and dielectric spectroscopy were employed to investigate the BP-III and TGB_A^* phases, as those techniques provide insights into their structural and dynamic properties. The ferroelectric behaviour of the SmC^* mesophase was investigated by electro-optics. The obtained results are discussed in relation to the molecular structures of the used materials.

1. Introduction

One of the unique characteristics of the chiral soft systems that may form self-organized, i.e., liquid crystalline, structures is the absence of a mirror symmetry. Chirality introduces a sense of handedness or "twist" to the molecular arrangement, which can lead to the formation of helical structures. Chiral calamitic liquid crystals (LC) can also exhibit a tendency to form layered smectic structures. Strongly chiral systems can result in the formation of helical structures due to chiral packing. These helices can compete with the natural tendency of molecules to form distinct layered structures [1, 2]. The helical arrangement allows small groups of molecules within local smectic layers to rotate, which in specific cases may lead to the emergence of frustrated phases [3]. Two notable subclasses of frustrated phases are the twist grain boundary (TGB) phases and the blue phases (BPs).

Over the past few years, the BP, which appears in chiral LCs in a limited temperature range close to the clearing temperature, has drawn a lot of attention [4–9]. The presence of high chirality causes BPs to appear in a temperature range between the chiral nematic phase (N^*) and the isotropic liquid phase. BPs are optically isotropic phases that exhibit a three-dimensional double-twist cylinder structure. There are three known types of BPs: BP-I (body-centred cubic symmetry), BP-II (simple cubic symmetry), and BP-III (amorphous and unidentified local structure) [10, 11]. Even though they lack of birefringence, they can still exhibit colourful selective reflection of circularly

*Corresponding author at: mkdnbu@yahoo.com

https://doi.org/10.24425/opelre.2024.151693
1896-3757/ Association of Polish Electrical Engineers (SEP) and Polish Academic of Sciences (PAS). Published by PAS

polarized visible light due to Bragg's reflection. Although BPs have many potential applications in high-performance optical and display devices, their narrow temperature range limited their practical applications [12–15]. Strategies like polymer stabilization, synthesis of new molecules, and nanoparticle insertion have been explored to expand their mesomorphic temperature range. Bent-core or hockey stick-shaped LCs are strong candidates for stabilizing BPs when appropriately doped with chiral dopants [3, 16]. The lactic acid derivatives can form various TGB phases by themselves and can be used effectively as chiral dopants to induce the frustrated mesophases [17–21]. The TGB phase is another type of frustrated mesophase. The TGB_A^* phase, predicted by Renn and Lubensky [22] and experimentally observed by Goodby *et al*. [1, 23], consists of Smectic-A* slabs connected by parallel screw dislocations at grain boundaries. The screw dislocations rotate at an angle about the nearby grain boundaries, relieving frustration and forming a helical superstructure and layer structure. So far, it has been reported that chiral-achiral mixtures can induce frustrated mesophases, leading to unique physical properties [24–26]. Comprehensive experimental investigations are needed to understand the formation mechanisms and exploring the relationship between molecular structure and mesomorphic properties of these complex mesophases and the specific rules of their formation in binary and multi-component mixtures.

2. Experimental

2.1. Materials

The chiral calamitic compound derived from the lactic acid (denoted as QVE8/5) was synthesized and purified at the Institute of Physics, Prague, Czech Republic [27–29]. The achiral hockey stick-shaped compound (denoted as H-22.5) was obtained from the Institute of Physical Chemistry, Martin Luther University, Halle, Germany [30]. The chemical structures and the related sequence of the mesophases are presented below.

Compound QVE8/5:
4-(octyloxy)phenyl 3-methoxy-4-((4-((2-(pentyloxy)-propanoyl)oxy)benzoyl)oxybenzoate

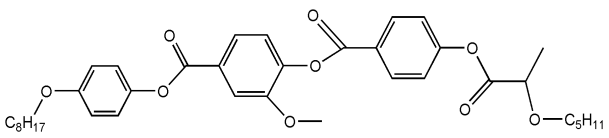

Mesophase: Iso **363.9K** N* **346.8K** SmC* **318.1K** Cr

Compound H-22.5:
(E)-4-((E-((3-(decyloxy)-2-methylphenyl)imino)methyl)-phenyl 3-(4-(dodecyloxy)phenyl)acrylate

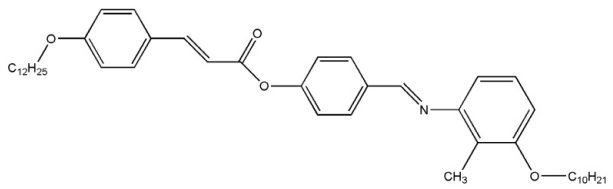

Mesophase: Iso **383.1K** N **382.7K** SmC_S **374.4K** SmC_A **347.2K** Cr

The achiral compound (H-22.5), which has an asymmetrical shape resembling a hockey stick, exhibits a stable phase sequence Iso-N-SmC_s-SmC_a-Cr upon cooling. The SmC_s and SmC_a are the tilted synclinic and anticlinic alignments of the molecules in adjacent layers of the tilted Smectic-C* phases, respectively; Cr stands for the crystal phase.

Two pure LC compounds in a specific ratio were carefully weighed using a high-precision digital balance (Mettler Toledo AB265-S). The compounds were then mixed for several hours using a continuous shaker machine set to a fixed temperature near their clearing points. Additionally, multiple heating and cooling cycles were conducted to ensure homogeneity. The following mole fractions of the hockey stick-shaped compound (H-22.5) in the chiral ferroelectric compound (QVE8/5) were prepared: $x_{H\text{-}22.5} = 0.162$, 0.25, 0.397, and 0.562.

2.2. Mesomorphic behaviour

The order of mesophases and their phase transition temperatures were determined using texture analysis with a polarizing optical microscope (Motic BA 300) equipped with an HCS302 hot stage. LC mixtures were filled in both planar and homeotropic 5 μm thick cells, then placed in a hot stage and focused to observe the textures and their changes in polarizing optical microscope (POM). The temperature of the hot stage was controlled using the mk1000 thermo-system (INSTEC, USA).

2.3. Birefringence

A planar aligned LC cell coated with indium tin oxide (ITO) conductive layers on the inner surface 5μm thick (from the Military University of Technology, Poland) was illuminated by a focused linearly polarized He-Ne laser beam($\lambda = 632.8$ nm). By placing the LC cell in a brass heater, the temperature of the cell was controlled and measured with a temperature controller (Eurotherm PID 2404) with an accuracy of ± 0.1 K. A photodiode interfaced with a precession multimeter, Keithley 2000 (U.S.A), was used to measure the intensity of the transmitted light: the data were recorded digitally with the help of a Matlab software. The experimental details for measuring birefringence using the optical transmission (OT) method were described in Refs. 31–33.

2.4. Static permittivity

The temperature-dependent static dielectric permittivity parameters ($\varepsilon_\parallel$ and $\varepsilon_\perp$) were measured using an Agilent 4294A impedance analyser with a relative accuracy of 0.08%. A small amount of sample was filled into an ITO-coated planarly (or homeotropically) aligned 5 μm thick cells. The cell was inserted into a hot stage HCS302 and connected with the mk1000 thermo-system to control and monitor the temperature. The details on the measurements were described in Refs. 34 and 35. The temperature-dependent cell capacitance value in various mesophases has been measured at a fixed frequency of 10 kHz and a signal voltage of 0.5 V. The values of both $\varepsilon_\parallel$ and $\varepsilon_\perp$ were used to calculate the temperature-dependent dielectric anisotropy and average permittivity over the entire mesomorphic range.

2.5. *Electro-optics*

Electro-optical measurements have been carried out using an arbitrary waveform generator Picotest (G5100A) and ferroelectric LC (FLC) voltage amplifier (F20A) to apply the square wave of voltage $V_{pp} = 36$ V, $f = 20$ Hz, on the sample-filled planar aligned cells with an active electrode area of ~ 25 mm^2. The polarization reversal technique was used to determine the spontaneous polarization (P_S) value. A current pulse was seen as the polarization was inverted by the applied field. A digital oscilloscope (DSO X2004A) that was properly interfaced with a computer recorded the current response. The detailed procedure was reported in Ref. 36.

2.6. *Dielectric spectroscopy*

The dielectric spectroscopy has been used to study the molecular relaxation processes and, consequently, to determine the orientation of the mesogens [37]. A precision LCR meter (Agilent 4294A) was used to measure the real (ε′) and imaginary (ε″) components of the complex permittivity on planar and homeotropically aligned samples. The cells containing the samples were placed in a thermally insulated hot-stage HCS302 (INSTEC). To find out the relaxation mechanism, the dielectric spectra were recorded within the frequency range from 40 Hz to 25 MHz with a maximum AC voltage of 0.5 V (rms). The experimental procedure for performing dielectric spectroscopy and analysing the obtained spectra has been discussed in detail in Ref. 38.

3. Result and discussion

3.1. *Texture observation*

The characteristics of textures observed in POM for a selected mixture, $x_{H\text{-}22.5} = 0.25$ are presented in Fig. 1(a)–(h). When the mixture was cooled from the isotropic phase at a rate of 0.5 K/min, it exhibited a uniform bluish texture under crossed polarizers. This bluish texture without domains is characteristic for the BP-III [Fig. 1(a)]. The transition from isotropic to BP-III is challenging to recognize due to the relatively small temperature ranged dark colour of the BP-III. Slight rotation of the analyser in both the clockwise and anticlockwise directions allowed

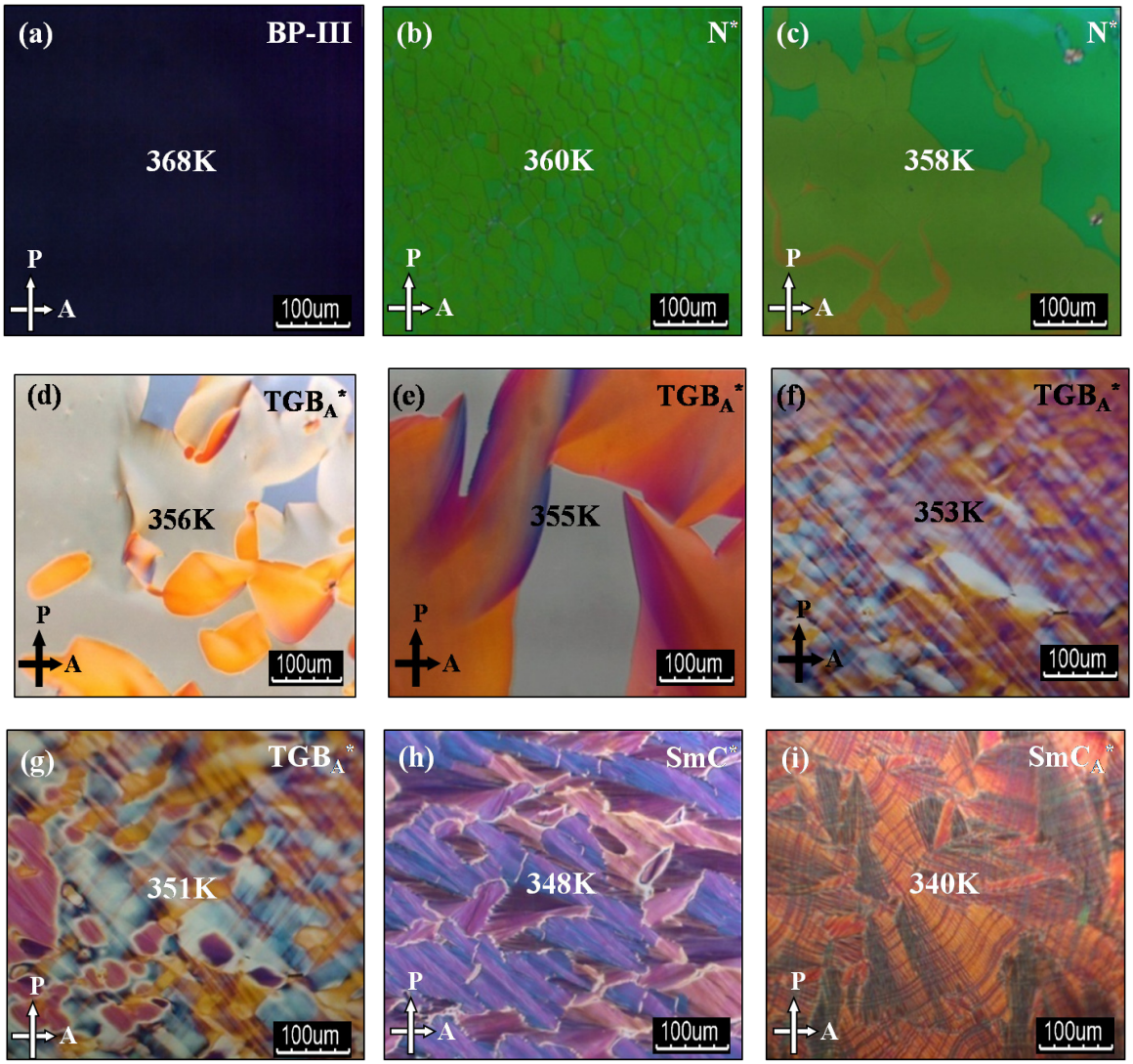

Fig. 1. Optical texture (crossed polarizers) observed at × 400 magnifications for a mixture with mole fraction $x_{H\text{-}22.5} = 0.25$ in planar alignment. (a) BP-III phase at 368 K, (b) N* phase at 360 K, (c) N* phase at 358 K, (d)TGB$_A^*$ phase at 356 K, (e) TGB$_A^*$ phase at 355 K, (f) TGB$_A^*$ phase at 353 K, (g)TGB$_A^*$phase at 351 K, (h) SmC* phase at 348 K, (i) SmC$_A^*$ phase at 340 K for $x_{H\text{-}22.5} = 0.562$. Arrows indicate the direction of the polarizers and analysers.

differentiation between BP-III and the isotropic phase. The BP-III phase exhibits weakly reflected light intensity unlike the isotropic phase that shows no reflection [39]. Under an external field of 40 V/μm, a slight change in BP-III texture has been observed with small domains or platelet textures appearing faintly within the uniform blue texture.

As the cooling continued, the BP-III phase transformed into a chiral nematic phase characterised by an oily streak pattern [Fig. 1(b)–(c)]. Upon further cooling, different colour domains appeared [Fig. 1(d)–(g)]. The existence of various colour domains is indicative of various twist states within the phase. This phase is identified as a twist inversion state, where specific colour domains initiate and rapidly grow. This phenomenon is like a twist inversion observed for other chiral compounds and mixtures [40–42]. With further decrease in temperature, the TGB_A^* phase transformed into the ferroelectric SmC^* phase [Fig. 1(h)] characterised by a typical broken fan texture. All the investigated mixtures exhibit similar phase sequences; however, the phase transition temperatures are different. For the mixture with $x_{H\text{-}22.5} = 0.562$, an additional anticlinic SmC_A^* phase is observed below the SmC^* phase which is characterised by striped fan texture as presented in Fig. 1(i).

In a homeotropic alignment, as temperature decreases, the N^* phase transforms into the frustrated TGB_A^* phase. The optical textures of the TGB_A^* phase are predominantly covered with a black region. The homeotropic texture of theTGB_A^* phase is like that of the SmA phase. Here, the orientation of the molecular director is parallel to the direction of the optic axis. This transformation is driven by the presence of a helix axis with a longer pitch length compared to the N^* phase. Frustrated phases, such as the BP-III and TGB_A^* phases, are typically found within a limited range of temperatures.

3.2. Phase diagram

Figure 2(a) presents a partial phase diagram of the binary system QVE8/5 + H-22.5. The phase transitions for the binary mixtures were determined using POM and static dielectric permittivity measurement during a cooling run. The pure achiral compound (H-22.5), shaped like a hockey stick, exhibits the N, tilted synclinic Smectic-C (SmC_s), and tilted anticlinic Smectic-C (SmC_a) phase, while the pure chiral compound QVE8/5 exhibits the chiral nematic (N^*) and the tilted ferroelectric Smectic-C (SmC^*) phases. The binary mixture of the chiral and achiral compounds induces the formation of the BP-III with the temperature range of about 2.5–6.2 K, and the TGB_A^* with the temperature range of about 1.8–6 K. The presence of the hockey stick-shaped mesogenic compound disrupts the chiral environment of the host chiral mesogen, leading to the formation of these frustrated phases (BP-III and TGB_A^*). Figure 2(b) displays the temperature ranges for the BP-III, N^*, and TGB_A^* phases for various concentrations of H-22.5. The width of the N^*phase decreases with an increase in molar concentration of H-22.5. In all four mixtures, the thermal ranges of BP-III and TGB_A^* phases initially increase and then decrease as the molar concentration of H-22.5 increases. Phase transition temperatures obtained from the texture analysis, static dielectric permittivity measurements and optical birefringence measurements are in good agreement with each other.

3.3. Optical birefringence

The phase retardation technique is being used in a planar cell to study the optical birefringence (Δn) of four mixtures and depicted in Fig. 3. This technique is useful for detecting and studying various phase transitions in LCs. This includes identifying phase transition temperatures such as the transition from BP-III to other phases. The detection of the phase transition to the BP-III phase was difficult using other methods (such as POM) because the texture remains almost dark (black) near the transition temperature. However, the phase retardation technique proved to be more efficient method for identifying the BP-III phase transition. An enhancement in transmitted intensity during the Iso-BP-III phase transition was detected, suggesting a change in molecular ordering.

This is possibly due to a strong surface anchoring of the planar aligned cell. As the nematic ordering increases during the BP-III-N^* phase transition, the birefringence (Δn) value also increases.

In all studied mixtures, a significant increase in birefringence is observed during the N^*-TGB_A^* phase transition.

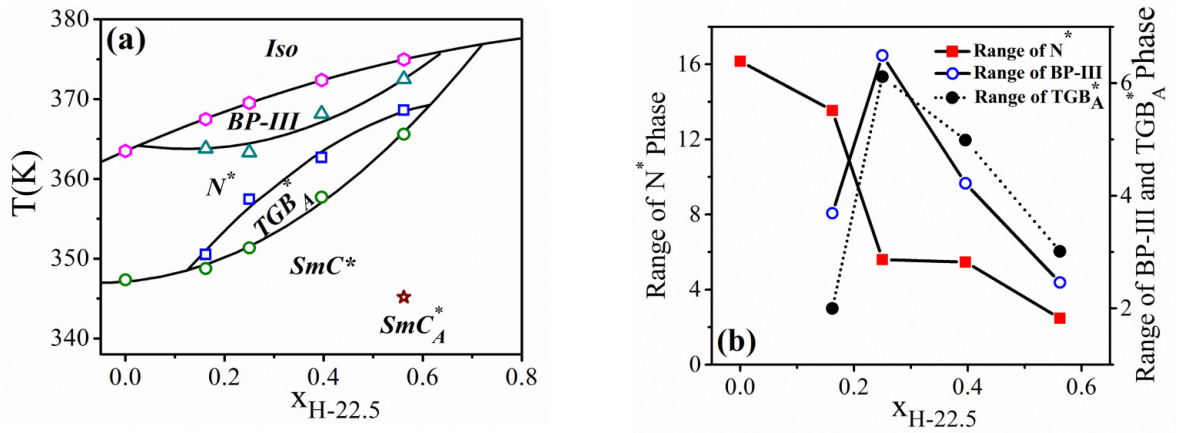

Fig. 2. (a) Partial phase diagram for the binary mixture of QVE8/5+H-22.5. $x_{H\text{-}22.5}$ defines as the mole fraction of the compound H-22.5. Iso – isotropic phase; BP-III – blue phase-III; N^* – chiral nematic phase; TGB_A^* – twist grain boundary SmA^* phase; SmC^* – chiral smectic-C* phase; SmC_A^* – antiferroelectric Smectic-C phase. (b) Temperature range variation of BP-III, N^*, TGB_A^* phase with concentration. Solid lines are drawn for eye guidance.

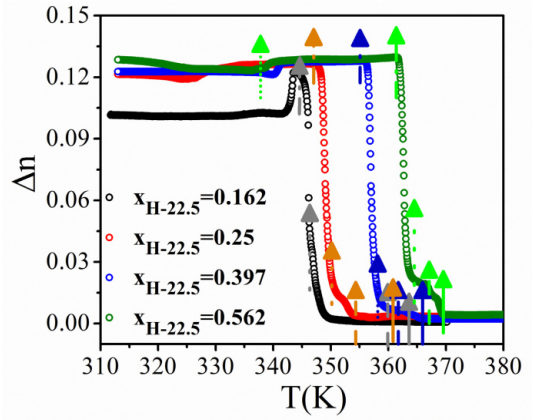

Fig. 3. Variation of optical birefringence (Δn) against temperature for all concentrations. Iso-BP-III: solid arrow; BP-III-N*: dashed arrow; N*-TGB$^*_A$: dotted arrow; TGB$^*_A$-SmC*: dash dotted arrow; SmC*-SmC$^*_A$: short dotted arrow.

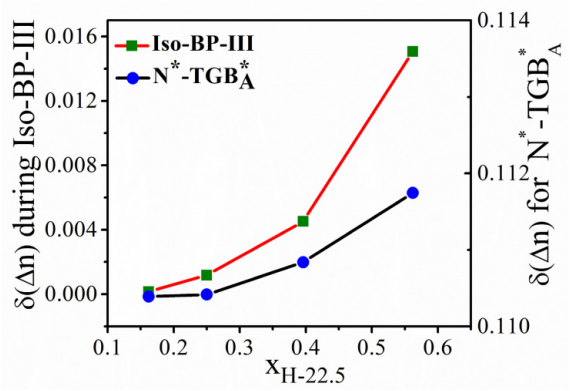

Fig. 4. Change in birefringence value ($\delta(\Delta n)$) against the molar concentration of compound H-22.5 ($x_{H-22.5}$) near the Iso-BP-III and N*-TGB$^*_A$ phase transition. Solid lines are drawn for eye guidance.

As the temperature is decreased, the helical structure of the cholesteric phase unwinds gradually, leading to a continuous expansion of the pitch length of the cholesteric helix. The phase transition to the TGB$^*_A$ phase involves twist inversion, leading to a sharp increase in birefringence. The birefringence eventually reaches a saturation value in the TGB$^*_A$ phase. Upon further cooling, a decrease in birefringence (Δn) is observed during the transition to the tilted ferroelectric SmC* (smectic) phase. The phase transition temperatures determined using the birefringence measurements are found to be in excellent agreement with those obtained from POM studies. In Fig. 4, the birefringence change $\delta(\Delta n)$ at the Iso-BP-III and N*-TGB$^*_A$ phase boundaries are examined with respect to the molar concentration of H-22.5. The analysis reveals that an increase in the concentration of H-22.5 leads to a greater relative birefringence change during these transitions.

3.4. *Static dielectric permittivity*

Figure 5(a)–(d) shows the temperature-dependent behaviour of permittivity components for different mixtures ($x_{H-22.5}$ = 0.162, 0.25, 0.397, 0.562) in planar (HG) and homeotropic (HT) cell arrangements. From Fig. 5(a), it is evident that, near the Iso-BP-III phase transition, the parallel component of permittivity ($\varepsilon_{\parallel}$) is greater than the

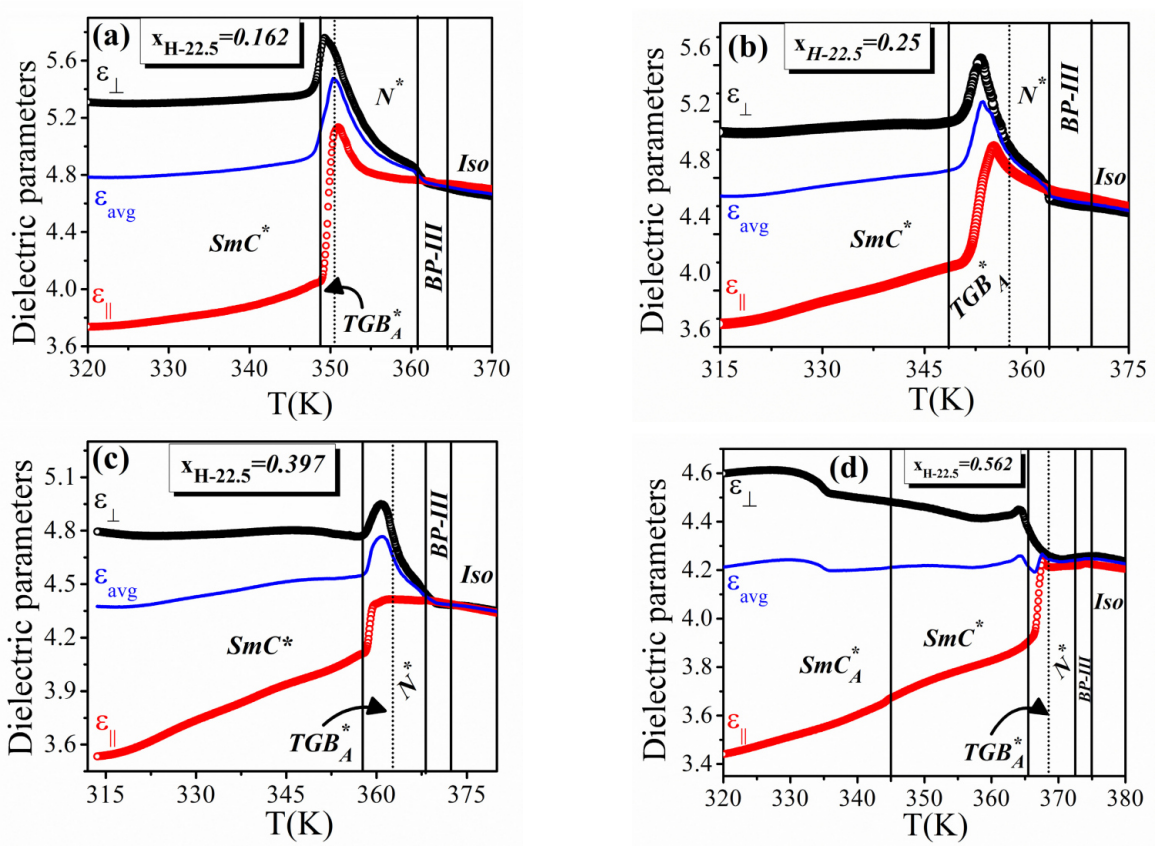

Fig. 5. Variation of dielectric parameters ($\varepsilon_{\parallel}$, $\varepsilon_{\perp}$, ε_{avg}) against temperature for four different molar concentrations of H-22.5. (a) $x_{H-22.5}$ = 0.162, (b) $x_{H-22.5}$ = 0.25, (c) $x_{H-22.5}$ = 0.397, (d) $x_{H-22.5}$ = 0.562. All the phase transition temperatures are indicated by vertical solid lines and the N*-TGB$^*_A$ phase transition is indicated by vertical dotted arrows.

perpendicular component ($\varepsilon_\perp$), indicating a positive dielectric anisotropy. As the system cools and transitions from the BP-III to the N^* phase, the perpendicular permittivity sharply increases compared to the parallel component, resulting in a crossover from positive to negative dielectric anisotropy. The$TGB_A^*$and SmC^* phases both exhibit negative dielectric anisotropy.

This negative anisotropy is attributed to the transverse dipole moment of the polar linking ester groups of QVE8/5 molecules, which enhances the permittivity perpendicular to the molecular long axis. Additionally, the transverse dipole moment of the hockey stick-shaped compound contributes to a higher $\varepsilon_\perp$ compared to $\varepsilon_\parallel$, along the long molecular axis. The other mixtures [Fig. 5(b)–(d)] show a similar trend. For a specific mixture ($x_{H\text{-}22.5} = 0.562$), the dielectric constants $\varepsilon_\perp$ and ε_{avg} slightly increase at the SmC^* to SmC_A^* transition. This increase from the SmC^*-SmC_A^* phase transition is attributed to the antiferroelectric soft mode and the vibration of azimuthal molecular motion [43–45] during the SmC^*-SmC_A^* phase transition. In the antiferroelectric phase, the absence of macroscopic polarization makes the Goldstone mode contribution inaccessible for dielectric measurement. However, the enhancement of the dielectric constant is attributed to the antiferroelectric soft mode and the vibration of azimuthal molecular motion.

Figure 6(a)–(b) shows how the dielectric anisotropy changes with temperature for all four investigated binary mixtures with definite concentrations. The magnitude of dielectric anisotropy ($\Delta\varepsilon$) decreases as the concentration of the hockey stick-shaped compound increases in the mixtures. For comparison, the anisotropy ($\Delta\varepsilon$) values at temperatures of 2 K below the Iso-BP-III and the N^*-TGB_A^* phase transition temperatures are plotted in Fig. 7.

In the BP-III phase, there is a positive $\Delta\varepsilon$ value. Initially, this positive $\Delta\varepsilon$ value increases with the concentration of $x_{H\text{-}22.5}$ ($x_{H\text{-}22.5} = 0.25$) and then decreases from 0.07 to 0.03. However, for the TGB_A^* phase, the magnitude of the negative $\Delta\varepsilon$ value decreases from 0.2 to 0.09 as the concentration of $x_{H\text{-}22.5}$ increases.

This indicates a change in the dielectric response and alignment of the LC molecules during these phase transitions. It is important to emphasize that, for the development of direct view and projected LC displays, it can be very advantageous to use LC materials having negative dielectric anisotropy [46, 47].

3.5. *Electro-optic*

The electric field-induced P_S in mixtures was measured using different types of AC input voltage waveforms (square and triangular). The ferroelectric ordering of the tilted SmC^* phase has been confirmed by detection of a single polarization peak in response to a triangular voltage waveform and the appearance of a current response hump in the square wave waveform. The values of P_S are shown in Fig. 8 as function of reduced temperature (T/T_C), where T_C is the transition temperature between the $TGB_A^*$and SmC^* phases. The ferroelectric SmC^* phase exhibits a rise in P_S values with T/T_C. The maximum P_S value of approximately 78 nC/cm² for a specific composition $x_{H\text{-}22.5} = 0.162$ has been observed. Higher tilt angle values and transverse dipole moment alignment of the SmC^* phase

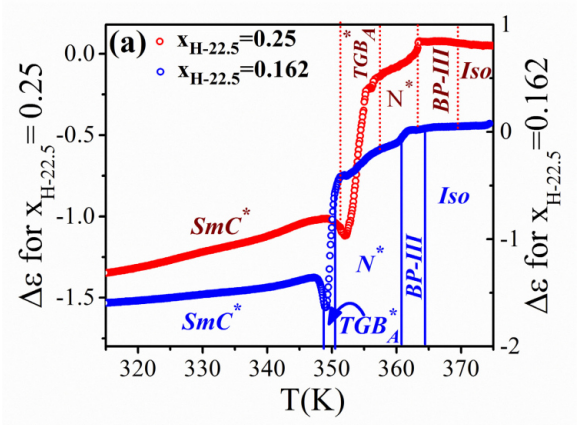

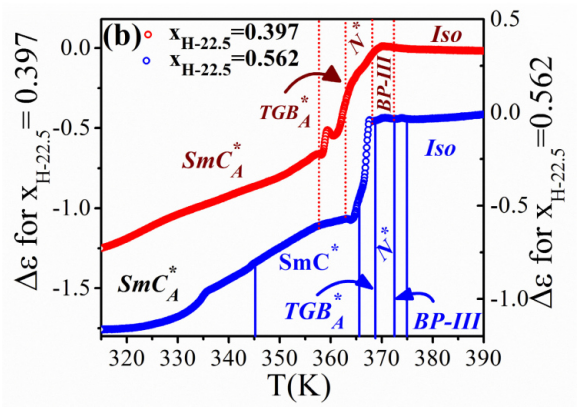

Fig. 6. Variation of dielectric anisotropy ($\Delta\varepsilon$) against temperature for (a) $x_{H\text{-}22.5} = 0.162$, 0.25, (b) $x_{H\text{-}22.5} = 0.397$, 0.562. All phase transition temperatures are indicated by vertical solid and dotted lines.

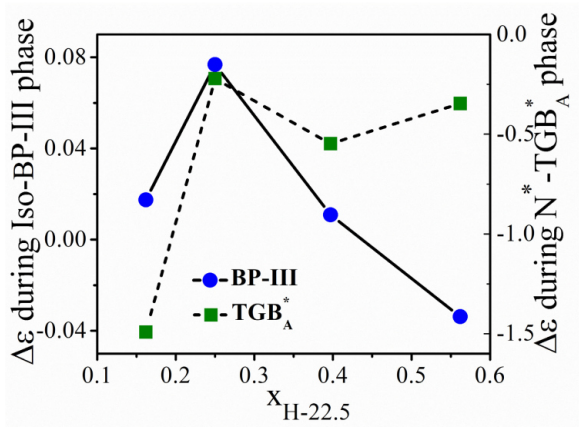

Fig. 7. Variation of dielectric anisotropy ($\Delta\varepsilon$) against molar concentration of H-22.5 ($x_{H\text{-}22.5}$) 2 K below the transition temperature of BP-III and TGB_A^*phases.

contribute to increased polarization. As temperature decreases, reorganization of the dipoles within the material occurs. This reorganization, along with electrostatic attraction between adjacent molecules, leads to higher P_S values at lower temperatures. The addition of an achiral hockey stick-shaped compound appears to reduce the effective P_S value. This reduction could be attributed to unfavourable alignment between dipole moments caused by the presence of the achiral compound. Differences in terminal chain length between chiral and achiral molecules may also contribute to the decrease in polarization value.

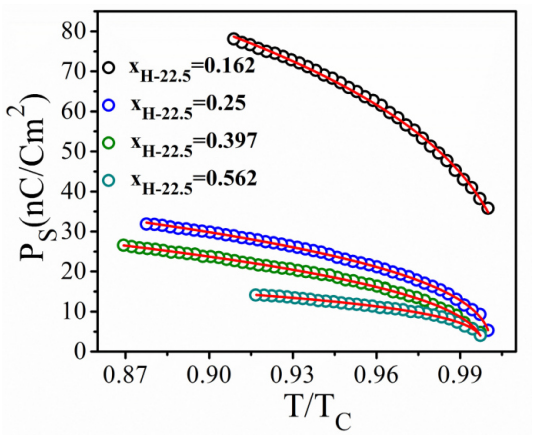

Fig. 8. Variation of P_S against T/T_C for $x_{H\text{-}22.5} = 0.162, 0.25, 0.397, 0.562$. The fitting results are represented by red solid lines using (1).

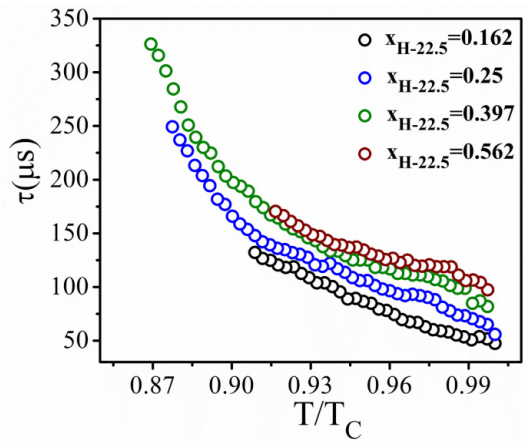

Fig. 9. Variation of response time (τ) against reduced temperature (T/T_C) for $x_{H\text{-}22.5} = 0.162, 0.25, 0.397, 0.562$.

The experimental data of the TGB_A^*-SmC^* phase transitions have been fitted using (1) [48, 49]:

$$P_S = P_0(T - T_C)^{\beta}. \quad (1)$$

Here, β presents the critical exponent, P_0 and β both are the movable parameters, and T_C is the temperature at which the TGB_A^*-SmC^* phase transition occurs. The red lines in Fig. 8 represent the fitted curves of (1) to the experimental data and Table 1 summarizes the fitted parameters.

The critical exponent (β) value extracted for the pure compound at the N^*-SmC^* phase transition is reported as 0.24 ± 0.001 [27]. This value is consistent with the tricritical mean-field model [50] suggesting that the N^*-SmC^*phase transition is weakly first order in nature. For various molar concentrations ($x_{H\text{-}22.5} = 0.162, 0.25, 0.397$, and 0.562), the critical exponent (β) values at the TGB_A^*-SmC^* phase transition is observed to increase. These β values range from 0.30 ± 0.003 to 0.40 ± 0.003. The extracted critical exponent values are very close to the theoretically predicted values (0.3125) from the three-dimensional Ising model [50].

The time (t_{10-90}) required to switch the current from 10% to 90% of its peak value at the hump of the repolarization curve is used to calculate the free relaxation time for the ferroelectric director. The relaxation time and t_{10-90} have the following relationship [51]:

$$\tau = \frac{t_{10-90}}{1.8}. \quad (2)$$

The values of response time (τ) as a function of T/T_C are shown in Fig. 9. As temperature decreases, τ shows enhancement throughout the SmC^* phase. Compared to the pure chiral compound, mixtures exhibit longer response times at specific temperatures as shown in Table 1. The presence of the hockey stick-shaped compound may hinder the movement of the chiral centre, leading to longer response times. The analysis of pure calamitic chiral compound has already been reported in Refs. 27 and 28.

The similarity between the experimentally extracted β values and the theoretically predicted values from the three-dimensional Ising model suggests that the TGB_A^*-SmC^* phase transition is second order in nature for all the studied mixtures. The addition of an achiral component to the chiral mesogen leads to a transition from a weakly first order N^*-SmC^* phase transition to a second order TGB_A^*-SmC^* phase transition. Therefore, the addition of an achiral component to the chiral mesogen drives the weakly first order N^*-SmC^* transition toward the second order TGB_A^*-SmC^* phase transition.

Figure 10 illustrates the relationship between the effective torsional η and T/T_C for various mixtures in the SmC^* phase. The plot demonstrates that as T/T_C decreases, effective torsional η of the mixtures in the SmC^* phase significantly increases.

Since η is directly related to τ, these two parameters exhibit a similar behaviour in response to changes in temperature.

The activation energy (E_a) is extracted using the following equation [52]:

$$\eta = \eta_0 \left(\frac{E_a}{k_\beta T}\right). \quad (3)$$

Table 1.
Parameters obtained through the use of (1)–(3) to fit the experimental P_S and η values for all mixtures in the SmC^* phase, including pure compounds at $T/T_C = 0.96$.

$x_{H\text{-}22.5}$	P_S(nC/cm^2)	P_0(nC/cm^2)	T_C	β	τ(μs)	η(mPas)	E_a(kJ/mol)
0	90.72	45.62 ± 0.002	346.8	0.24 ± 0.001	70.90	469.58	71.39
0.162	62.41	23.44 ± 0.18	342.46	0.31 ± 0.002	76.10	354.53	49.53
0.25	21.26	7.60 ± 0.05	351.28	0.36 ± 0.002	97.64	150.30	46.93
0.397	16.44	5.54 ± 0.06	351.46	0.40 ± 0.003	116.84	142.52	39.98
0.562	11.29	5.12 ± 0.04	360.43	0.30 ± 0.003	125.29	104.60	32.66

Here, the parameter T present the absolute temperature and k_β is the Boltzmann's constant. The slope of the linear region in the plot can be used to determine the activation energy. The activation energy is extracted from the slope of the linear region. The extracted E_a values for various mixtures, including pure compounds, are listed in Table 1. The inset of Fig. 10 displays the representative fit for the binary mixture $x_{H\text{-}22.5} = 0.25$.

Anchoring energy is crucial in FLC materials. It affects molecular alignment and memory effects. There are two primary types of anchoring strengths: polarization (W_P) and dispersion (W_D). Polarization anchoring strength arises from the competition between the surface dipole moments and the persistent dipole moments in the FLC phases. Dispersion anchoring strength, on the other hand, results from non-electrostatic interactions between the surface and the LC molecules, primarily due to Van der Waals forces.

The relationship between the response time and the dispersion anchoring strength coefficient (W_D) can be expressed as [53–56]:

$$W_D = \frac{\eta d}{4\tau} \tag{4}$$

In Fig. 11(a) and (b), the reduced temperature dependency of W_D and W_P are shown. As the temperature increases, both W_P and W_D exhibit a similar pattern of decreasing until they reach their minimum values at the TGB_A^*-SmC^*phase transition for all the mixtures. The decreasing trend of both $W_P$and W_D with rising temperature suggests that the enthalpy of molecules steadily increases with temperature. This increase in enthalpy could lead to the breaking of barriers [57] that prevent molecular interactions, resulting in a decrease in both anchoring strengths. The value of W_P is slightly higher than that of W_D, which is evident from comparing Fig. 11(a) and (b). This observation could imply that compounds with higher P_S values might contribute more to W_P. In other words, molecules with greater intrinsic polarization tendencies may have a stronger influence on the alignment of the LC material.

The P_S, the W_D, and the W_P are connected as follows [53–56]:

$$W_P = \sqrt{P_S \sqrt{W_D}}. \tag{5}$$

3.6. *Dielectric spectroscopy*

The dielectric spectroscopy was used to investigate the relaxation modes presented in the binary mixtures. It involves measuring the real (ε′) and imaginary (ε") parts of the complex permittivity as a function of frequency. This response provides insights into how molecules within the system respond to an electric field, which in turn reveals important information about their behaviour and interactions. The logarithmic plot of the imaginary part of the complex permittivity *vs*. frequency allows for a clear visualization and identification of these relaxation modes. One representative mixture, $x_{H\text{-}22.5} = 0.25$, is shown in Figs. 12(a)–(c) and 13(a)–(c) for both homeotropic and planar element. In the BP-III phase, a distinct relaxation mode appears at the high frequency region around 45 KHz.

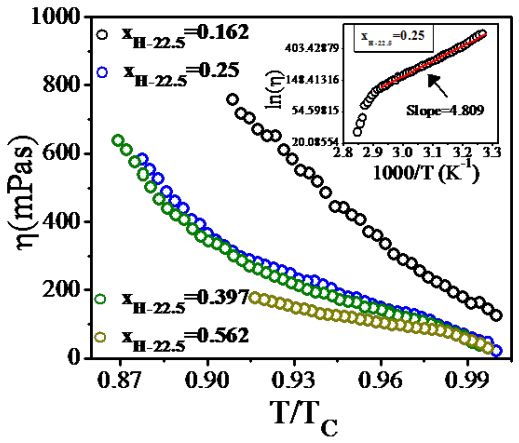

Fig. 10. Variation of effective torsional bulk viscosity (η) against (T/T_C for $x_{H\text{-}22.5} = 0.162, 0.25, 0.397, 0.562$. The linear fit to experimental data with (3) is shown in the inset for $x_{H\text{-}22.5} = 0.25$.

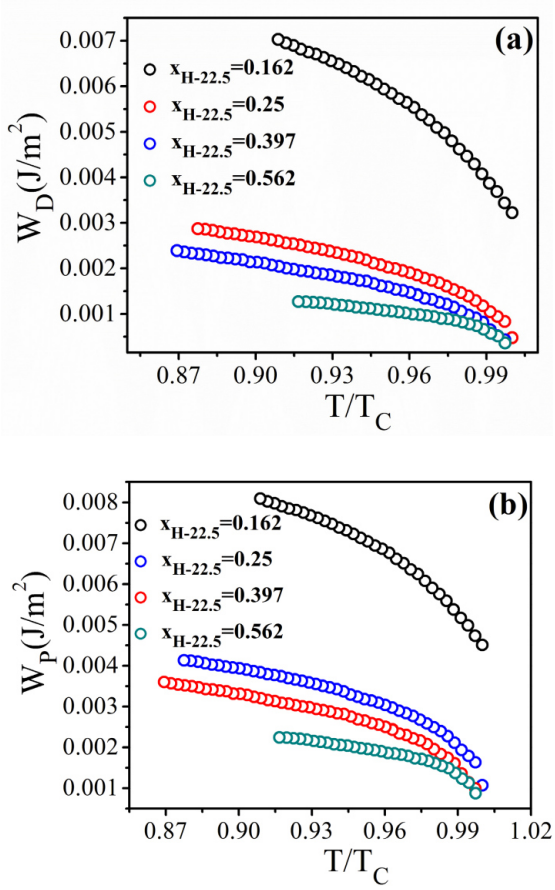

Fig. 11. Variation of (a) dispersion anchoring energy coefficient (W_D) and (b) polarization anchoring energy coefficient (W_P) against T/T_C for $x_{H\text{-}22.5} = 0.162, 0.25, 0.397, 0.562$ in the SmC^* phase.

On the other hand, the relaxation frequency in the TGB_A^* phase is positioned between the soft mode and the Goldstone mode. This suggests that an electric field will cause the amplitude of the tilt angle to fluctuate, making the soft mode (~ 40 KHz) observable in the TGB_A^* phase. While in the SmC^* phase, the Goldstone mode arises due to phase fluctuations of long molecular axes at lower frequencies (typically around 1–3 kHz). In planar alignment

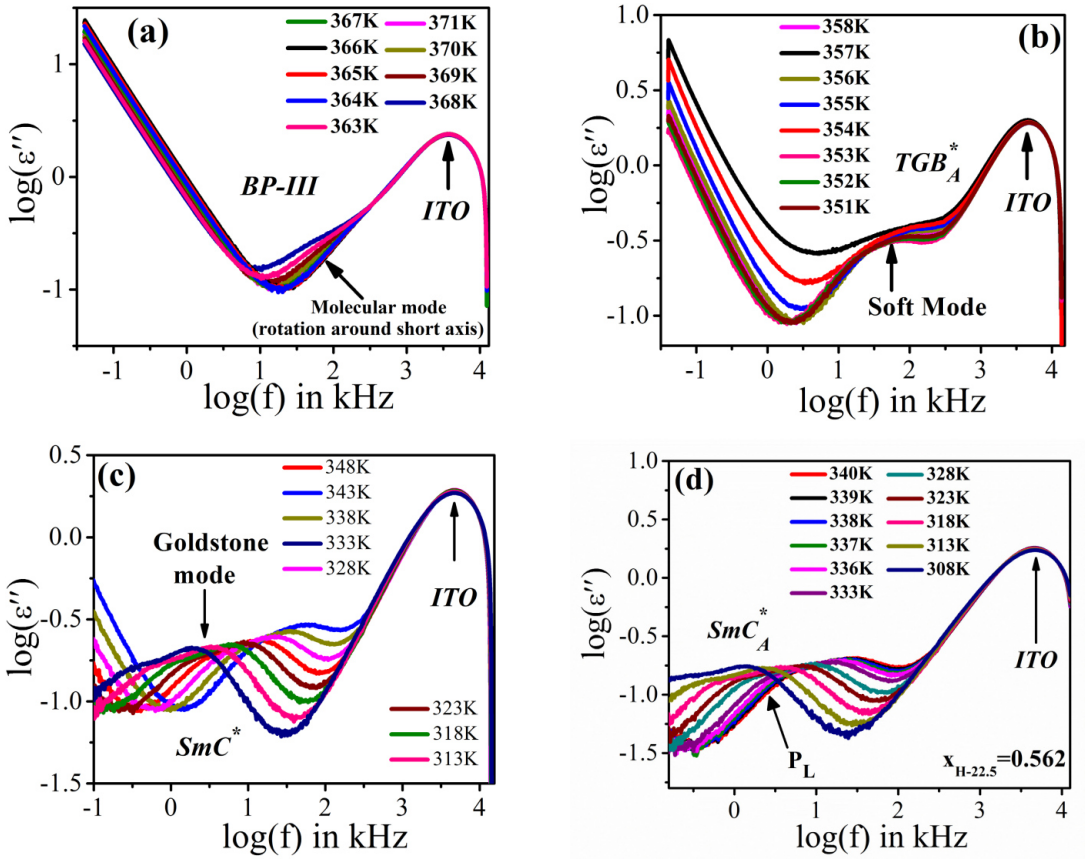

Fig. 12. Logarithmic plot of the imaginary part of complex permittivity (ε'') with frequency for $x_{H\text{-}22.5} = 0.25$ at different temperatures near (a) BP-III, (b) TGB_A^*, (c) SmC^*, (d) SmC_A^* phases in homeotropic alignment.

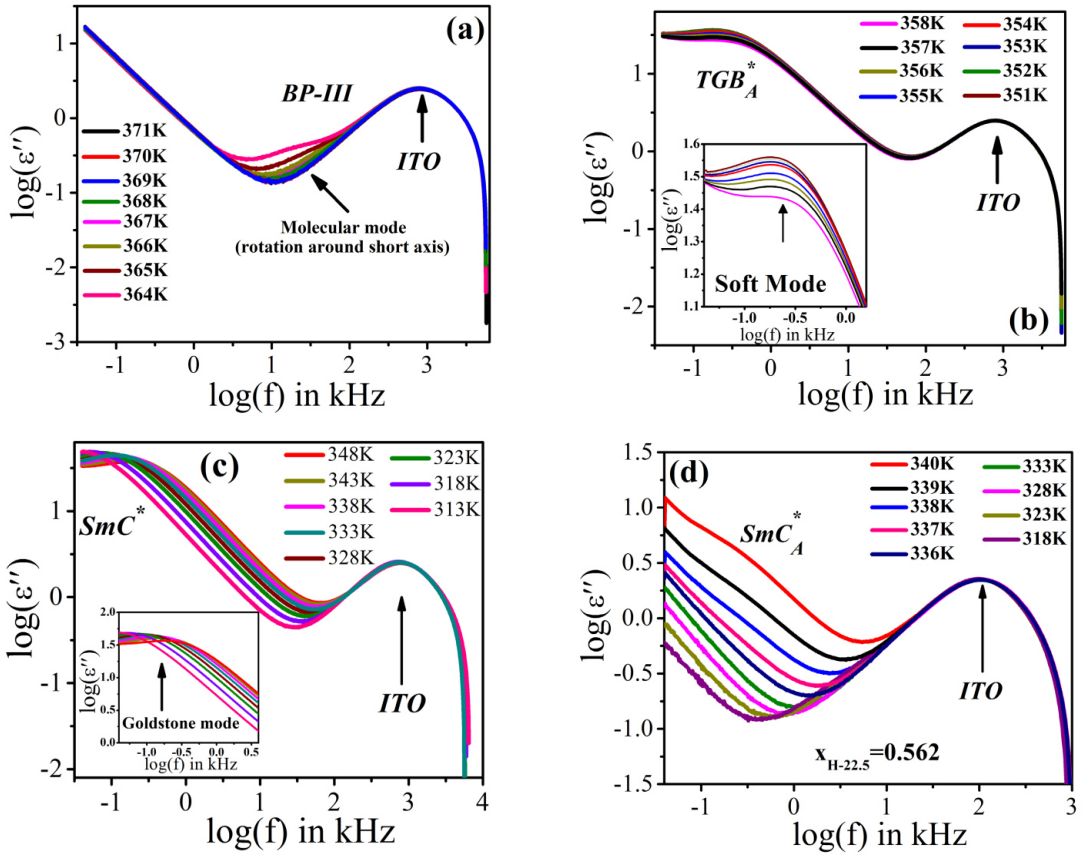

Fig. 13. Logarithmic plot of the imaginary part of complex permittivity (ε'') with frequency for $x_{H\text{-}22.5} = 0.25$ at different temperatures near (a) BP-III, (b) TGB_A^*, (c) SmC^*, (d) SmC_A^* phases for $x_{H\text{-}22.5} = 0.562$ in planar alignment.

[Fig. 12(c)], a sharp increase found due to helix unwinding was observed in SmC* exhibiting Goldstone mode with a high value of permittivity. The dielectric relaxation modes in the SmC^*_A for $x_{H\text{-}22.5} = 0.562$ are presented in Figs. 12(d) and 13(d). In the SmC^*_A phase, only one relaxation mode is observed in the low-frequency range, i.e., P_L mode which arises due to reorientation of the molecules around the molecular axis in phase. In the high frequency region, another mode P_H due to the anti-phase motion of adjacent molecular pair is not detected because this mode is suppressed by the Goldstone mode present in the adjacent high temperature phase (SmC* phase) [58–60]. Another mode is detected in the higher-frequency region. This higher-frequency mode is attributed to the finite resistivity of the ITO layers in measuring cells. One notable observation is the similarity in the appearance of the molecular mode across all the investigated mixtures.

Dielectric strength and relaxation frequency are the key parameters that characterise the relaxation modes. The Havriliak-Negami equation [61] is employed to fit the imaginary part of complex permittivity (ε'') data, allowing for the extraction of these parameters. In dielectric study of a representative mixtures in homeotropic geometry [Fig. 12(c)], two distinct relaxation modes (excluding ITO mode) are observed at SmC* phase for all investigated mixtures. Figure 14(a)–(b) illustrates that the dielectric strength undergoes a significant increase near the Iso-N* phase region and decreases after the N*-SmC* phase transition via TGB^*_A phase. Among all the studied mixtures, $x_{H\text{-}22.5} = 0.162$ exhibits the highest dielectric strength (~ 1.52) and the lowest relaxation frequency (~ 7.82 kHz) near the TGB^*_A-SmC* phase transition. A similar trend has been found in the values of dielectric strength for the second relaxation mode ($\delta\varepsilon_2$) in higher frequency region [inset in Fig. 14(a)–(b)] with nominal temperature dependency. The relaxation frequency shows increasing trend with increasing temperature [Fig. 14(a)–(b)]. Below the TGB^*_A region, the relaxation frequency (f_{r1}) due to $\delta\varepsilon_1$ for all concentrations lies between 120 kHz and 2 Hz. From N*-TGB^*_A transition, it increases rapidly and shows a value of ~ 167 kHz near BP-III-Iso phase transition in a 0.25 molar concentration. The maximum value of f_{r2} near the BP-III-Iso phase transition is ~ 500 kHz for 0.397 molar concentrations. The relaxation times (τ_1 and τ_2) show reverse trend of frequency with the variation of concentration. In lower temperatures, they show maximum with 1 ms in TGB^*_A phase and 0.8 ms in the BP-III phase region for 0.562 molar concentration which are quite low values due to easy switching of the molecules.

In the TGB^*_A phase, the relaxation frequency of this mode decreases linearly upon cooling, suggesting soft mode-like behaviour. Dielectric strength is low in the TGB^*_A phase, but builds up as the compound enters the smectic phase, attains a maximum and then decreases. As the temperature is reduced beyond the TGB^*_A-SmC* transition, $\delta\varepsilon_1$ becomes lower. There is a possibility that this relaxation process is a Goldstone mode. In the vicinity of the SmC*-SmC^*_A transition temperature, the dielectric strength of the Goldstone mode decreases rapidly with decreasing temperature and is registered into SmC^*_A phase. The relaxation frequency of this mode shows a strong temperature dependence following Arrhenius behaviour

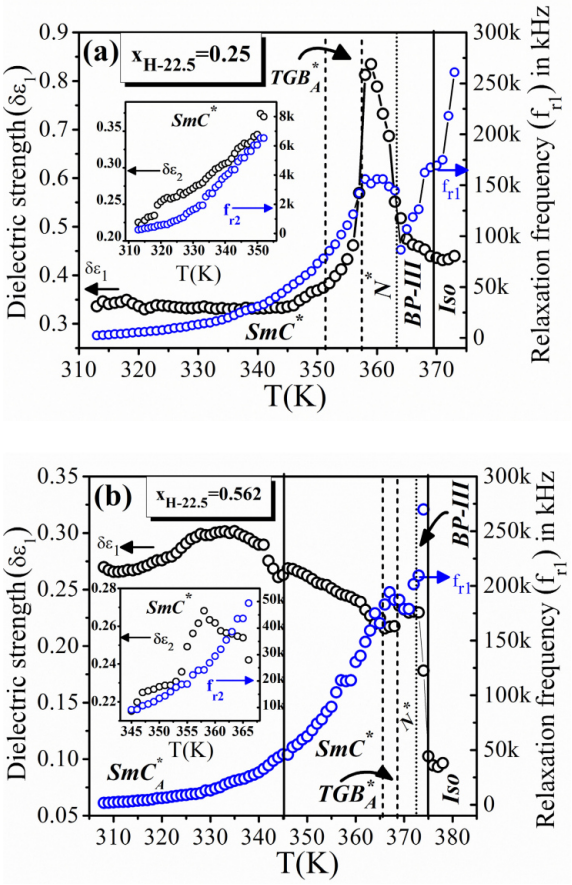

Fig. 14. Temperature variation of dielectric strength ($\delta\varepsilon_1$, $\delta\varepsilon_2$) and relaxation frequency (f_{r1}, f_{r2}) for (a) $x_{H\text{-}22.5} = 0.25$, (b) $x_{H\text{-}22.5} = 0.562$ in homeotropic alignment.

[62]. However, dielectric strength of this mode remains constant with temperature. This particular mode corresponds to rotation of molecules around their short axes.

For planar alignment [Fig. 13(a)–(d)], one distinct relaxation mode (excluding ITO mode) is observed across all mesophases for all investigated mixtures. The presence of Goldstone mode in the low-frequency region (~ 200 Hz) has the highest dielectric strength and strong temperature dependence. Figure 15(a)–(c) shows the temperature variation of dielectric strength, relaxation time, and relaxation frequency in the SmC* temperature region phase for all mixtures in planar alignment. The maximum value (at a 0.162 molar concentration) of dielectric strength is ~ 82 in SmC* phase (325 K). The values of dielectric strength decreases with increasing concentrations and having minimum value (~ 42 in SmC* phase) for a 0.562 molar concentration. The relaxation frequencies increase rapidly with temperature and show value ~ 450 KHz near BP-III-Iso phase transition in a 0.162 molar concentration. The relaxation times [Fig. 15(b)] show reverse trend of frequency with the variation of concentration. In lower temperatures, they show a maximum with 3.16 ms for 0.397 molar concentrations. All the mixtures show low relaxation times of the order of ~ 3–0.3 msec which makes them promising materials for application in high-speed optoelectronic device.

The temperature dependence of the relaxation frequency is analysed further through the least squares fit of log(f)

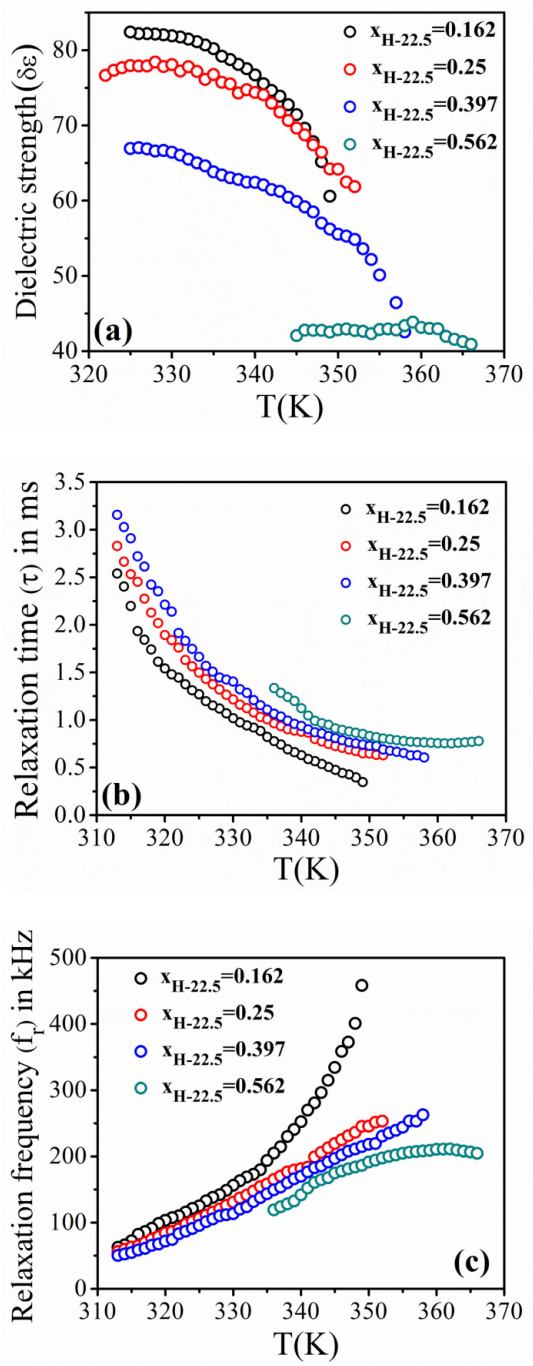

Fig. 15. Temperature variation of (a) dielectric strength (δε), (b) relaxation time (τ), and (c) relaxation frequency (f_r) of the Goldstone mode (SmC*phase) for all four binary mixtures in planar alignment, $x_{H-22.5}$ = 0.162, 0.25, 0.397, 0.562.

with 1/T, resulting in a straight-line relationship [63]. E_a corresponding to various phases is calculated from this analysis in homeotropic alignment. Activation energy is related to the amount of energy that is required to cross these potential barriers. The calculated activation energies for the SmC*, TGB_A^* and BP-III phases are shown in Table 2.

4. Conclusions

In this work, the results of an experimental study involving binary mixtures of chiral and achiral compounds, particularly focusing on their mesomorphic behaviour, optical, dielectric, and electro-optical properties are presented. Four binary mixtures were designed using varying molar concentrations ($x_{H-22.5}$ = 0.162, 0.25, 0.397, 0.562) of an achiral hockey stick-shaped compound (H-22.5) in chiral calamitic mesogen (QVE8/5). The chiral calamitic compound displayed a phase sequence of Iso-N*-SmC*-Cr, while the achiral compound exhibited a narrow temperature range of the nematic and two tilted smectic phases (synclinic smectic-C and anticlinic smectic-C). The addition of the achiral compound in a chiral matrix resulted in an induction of induced frustrated phases, including BP-III and TGB_A^* phases, between isotropic to N* and N* to SmC* phase transitions, respectively. The addition of the hockey stick-shaped achiral compound disrupted the helix orientation of the chiral compound, leading to the induction of frustrated phases with increased pitch length. The introduction of an achiral compound reduces the twisting power of the chiral mesogen, leading to a reduced range of the N* phase. This affects the stability and range of BP-III and TGB_A^* phases. The thermal stability of BP-III and TGB_A^* phases initially increases and then decreases with higher concentrations of the achiral compound. The maximum thermal stability of BP-III and TGB_A^* phases is observed at ~ 6.2 K and ~ 6 K, respectively, for definite molar concentration of $x_{H-22.5}$ = 0.25. The presence of small value of birefringence in BP-III suggests that it is not purely isotropic under strong surface anchoring. The TGB_A^* phase experiences twist inversion and higher birefringence. Δε exhibited a sign inversion, transitioning from positive to negative as the concentration of the achiral compound increased. P_S values decreased, while τ and effective torsional η increased compared to the pure chiral compound [34]. The N*-SmC* phase transition in the pure chiral compound was weakly first order, but the induction of the TGB_A^* phase transformed the TGB_A^*-SmC* phase transition to second order.

Dielectric spectroscopy revealed molecular modes in BP-III, due to the rotation of molecules around a short axis.

Table 2.
Activation energies (in kJ/mol) calculated for all the concentration in SmC_A^*, SmC*, TGB_A^*, and BP-III phase.

$x_{H-22.5}$	SmC_A^* (kJ/mol)	SmC* (kJ/mol)	TGB_A^* (kJ/mol)	BP-III (kJ/mol)
0.162	–	44.23	38.12	61.82
0.25	–	38.64	56.63	64.08
0.397	–	35.04	44.79	62.75
0.562	39.16	27.20	41.52	56.39

The intermediate TGB_A^* phase, on the other hand, represents a transition from a soft mode in N^* to the Goldstone mode in SmC^*phase. f_r and δε of the Goldstone mode in the SmC^*phase decrease slightly with molar concentration of the achiral compound. The reported experimental results provide insights into the molecular structure, mesomorphic properties, and phase transitions in chiral-achiral binary LC systems. This understanding is valuable for studying stable TGB phase formation targeted for advanced self-organizing and soft matter systems.

Authors' statement

Research concept and design, M.K.D.; collection and/or assembly of data, S.M.; data analysis and interpretation, S.M., P.B., and M.K.D.; writing the article, S.M., P.B., and M.K.D; critical revision of the article, M.K.D., A.B., and V.H.; final approval of article, M.K.D. and A.B.

Acknowledgements

This work was supported by the funds granted to the UGC-DAE CSR through a Collaborative Research Scheme (CRS) (Project no.: CRS/2021-22/01/351) and by the Czech Science Foundation project no. CSF23-42944L. We are thankful to Prof. Wolfgang Weissflog from Martin Luther-University (Germany) for providing the achiral hockey stick-shaped compound (H-22.5).

References

[1] Goodby, J. W. *et al*. Characterization of a new helical smectic liquid crystal. *Nature* **337**, 449–452 (1989). https://doi.org/10.1038/337449a0

[2] Lagerwall, J. P. F. & Giesselmann, F. Current topics in smectic liquid crystal research. *Chem. Phys. Chem*. **7**, 20–45 (2006). https://doi.org/10.1002/cphc.200500472

[3] Lee, M. *et al*. Liquid crystalline blue phase I observed for a bent-core molecule and its electro-optical performance. *J. Mater. Chem*. **20**, 5813–5816 (2010). https://doi.org/10.1039/C0JM01087A

[4] Wright, D. C. & Mermin, N. D. Crystalline liquids: the blue phases. *Rev. Mod. Phys*. **61**, 385–432 (1989). https://doi.org/10.1103/RevModPhys.61.385

[5] Liquid Crystalline Functional Assemblies and Their Supramolecular Structures. in *Structure and Bonding* (ed. Kato, T.) 128 (Springer, New York, 2008).

[6] Otón, E., Netter, E., Nakano, T., Katayama, Y. D. & Inoue, F. Monodomain blue phase liquid crystal layers for phase modulation. *Sci. Rep*. **7**, 44575 (2017). https://doi.org/10.1038/srep44575

[7] Otón, E. *et al*. Orientation control ofideal blue phase photonic crystals. *Sci. Rep*. **10**, 10148 (2020). https://doi.org/10.1038/s41598-020-67083-6

[8] Otón, E., Morawiak, P., Gaładyk, K., Oton, J. M. & Piecek, W. Fast self-assembly of macroscopic blue phase 3D photonic crystals. *Opt. Express* **28**, 18202–18211 (2020). https://doi.org/10.1364/OE.393197

[9] Orzechowski, K. *et al*. Achiral nanoparticle-enhanced chiral twist and thermal stability of blue phase liquid crystals. *ACS Nano* **16**, 20577–20588 (2022). https://doi.org/10.1021/acsnano.2c07321

[10] Crooker, P. P. Blue Phases. in *Chirality in Liquid Crystals* (eds. Kitzerow, H. S. & Bahr, C.) 186–222 (Springer, New York, 2001).

[11] Kikuchi, H. Liquid crystalline blue phases. *Struct. Bond.* **128**, 99–117 (2008). https://doi.org/10.1007/430_2007_075

[12] Rao, L., Ge, Z. & Wu, S. T. Viewing angle controllable displays with a blue-phase liquid crystal cell. *Opt. Express* **18**, 3143–3148 (2010). https://doi.org/10.1364/OE.18.003143

[13] Lu, S.-Y. & Chien, L.-C. Electrically switched color with polymer-stabilized blue phase liquid crystalls. *Opt. Lett*. **35**, 562–564 (2010). https://doi.org/10.1364/OL.35.000562

[14] *Liquid Crystals – Applications and Uses*. *Vol. 2*. (ed. Bahadur, B.) (Litton Systems Canada, 1991). https://doi.org/10.1142/1299

[15] Gray, G. W. & Kelly, S. M. Liquid crystals for twisted nematic display devices. *J. Mater. Chem*. **9**, 2037–2050 (1999). https://doi.org/10.1039/A902682G

[16] Taushanoff, S. *et al*. Stable amorphous blue phase of bent-core nematic liquid crystals doped with a chiral material. *J. Mater. Chem.* **20**, 5893–5898 (2010). https://doi.org/10.1039/C0JM00690D

[17] Kašpar, M. *et al*. New chlorine-substituted liquid crystals possessing frustrated TGB_A and SmQ phases. *Liq. Cryst*. **35**, 641–651 (2008). https://doi.org/10.1080/02678290802056212

[18] Cigl, M. *et al*. Photosensitive chiral self-assembling materials: significant effects of small lateral substituents. **4**, 5326–5333 (2016). https://doi.org/10.1039/C6TC01103A

[19] Poryvai, A., Bubnov, A., Pociecha, D., Svoboda, J. & Kohout, M. The effect of terminal n-carboxylate chain length on self-assembling and photosensitive properties of lactic acid derivatives. *J. Mol. Liq.* **275**, 829–838 (2019). https://doi.org/10.1016/j.molliq.2018.11.058

[20] Bubnov, A. *et al.* Eutectic behaviour of binary mixtures composed by two isomeric lactic acid derivatives. *Ferroelectrics* **495**, 105–115 (2016). https://doi.org/10.1080/00150193.2016.1136776

[21] Das, B. *et al*. Mesomorphic and structural properties of liquid crystal possessing a chiral lactate unit. *J. Mol. Struct.* **1013**, 119–125 (2012). https://doi.org/10.1016/j.molstruc.2012.01.017

[22] Renn, S. R. & Lubensky, T. C. Abrikosov dislocation lattice in a model of the cholesteric to smectic-A transition. *Phys. Rev. A* **38**, 2132–2147 (1988). https://doi.org/10.1103/PhysRevA.38.2132

[23] Goodby, J. W. *et al.* A new molecular ordering in helical liquid crystals. *J. Am. Chem. Soc*. **111**, 8119–8125(1989). https://doi.org/10.1021/JA00203A009

[24] Dierking, I. A review of textures of the TGB_A^* phase under different anchoring geometries. *Liq. Cryst*. **26**, 83–95 (1999). https://doi.org/10.1080/026782999205588

[25] Sahoo, R. & Dhara, S. A short review on the rheology of twist grain boundary-A and blue phase liquid crystals. *Fluids* 3, 1–15 (2003). https://doi.org/10.3390/fluids3020026

[26] Chakraborty, S. *et al*. Induced frustrated twist grain boundary liquid crystalline phases in binary mixtures of achiral hockey stick-shaped and chiral rod-like materials. *J. Mater. Chem. C* **7**, 10530–10543 (2019). https://doi.org/10.1039/C9TC02917F

[27] Barman, B., Das, B., Das, M. K., Hamplova, V. & Bubnov, A. Effect of molecular structure on dielectric and electro-optic properties of chiral liquid crystals based onlactic acid derivatives. *J. Mol. Liq*. **283**, 472–481 (2019). https://doi.org/10.1016/j.molliq.2019.03.071

[28] Das, M. K., Barman, B., Das, B., Hamplova, V. & Bubnov, A. Dielectric properties of chiral ferroelectric liquid crystalline compounds with three aromatic rings connected by ester groups. *Crystals* **9**, 473 (2019). https://doi.org/10.3390/cryst9090473

[29] Bubnov, A. *et al.* Effect of lateral methoxy substitution on mesomorphic and structural properties of ferroelectric liquid crystals. *Liq. Cryst.* **35**, 1329–1337 (2008). https://doi.org/10.1080/02678290802585525

[30] Chakraborty, A. *et al*. New hockey stick compounds with a lateral methyl group showing nematic, synclinic and anticlinic smectic C phases. *Liq. Cryst*. **38**, 1085–1097 (2011). https://doi.org/10.1080/02678292.2011.596227

[31] Prasad, A. & Das, M. K. Optical birefringence studies of a binary mixture with the nematic-smectic-A_d-re-entrant nematic phase sequence. *J. Phys. Conds. Matter* **22**, 195106 (2010). https://doi.org/10.1088/0953-8984/22/19/195106

[32] Sarkar, G. K., Das, B., Das, M. K., Baumeister, U. & Weissflog, W. Structural investigations of a non-calamitic shaped liquid crystalline compound showing unusual phases. *Mol. Cryst. Liq. Cryst.* **540**, 188–195 (2011). https://doi.org/10.1080/15421406.2011.568840

[33] Sarkar, S. K. & Das, M. K. Critical behaviour at the nematic-smectic A phase transition in a binary mixture showing induced nematic phase. *RSC Adv*. **4**, 19861–19868 (2014). https://doi.org/10.1039/C4RA00439F

[34] Chakraborty, A., Das, M. K., Das, B., Baumeister, U. & Weissflog, W. Optical, dielectric and visco-elastic properties of a few hockey stick-shaped liquid crystals with a lateral methyl group. *J. Mater. Chem. C* 1, 7418–7429 (2013). https://doi.org/10.1039/C3TC31565G

[35] Sarkar, S. K. & Das, M. K. Critical behavior of dielectric permittivity in the vicinity of nematic–isotropic and smectic–nematic phase transitions in smectogenic binary mixtures. *Fluid Ph. Equilibria* **365**, 41–49 (2014). https://doi.org/10.1016/j.fluid.2013.12.010

[36] Pramanik, A., Das, M. K., Das, B., Zurowska, M. & Dabrowski, R. Electro-optical properties of a new series of fluorinated antiferroelectric orthoconic liquid crystalline esters. *Liq. Cryst*. **42**, 412–421 (2015). https://doi.org/10.1080/02678292.2014.996792

[37] Chaudhury, A., Malik, P., Mehra, R. & Raina, K. K. Influence of ZnO nanoparticle concentration on electro-optic and dielectric properties of ferroelectric liquid crystal mixture. *J. Mol. Cryst*. **188**, 230–236 (2013). https://doi.org/10.1016/j.molliq.2013.09.020

[38] Chakraborty, S., Das, M. K., Keith, C. & Tschierske, C. Study of ferro-and anti-ferroelectric polar order in mesophases exhibited by bent core mesogens. *Mater. Adv*. **1**, 3545–3555 (2020). https://doi.org/10.1039/D0MA00678E

[39] Gim, M.-J., Han, G., Choib, S.-W. & Yoon, D. K. Thermal phase transition behaviours of the blue phase of bent-core nematogen and chiral dopant mixtures under different boundary conditions. *Soft Matter* **10**, 8224–8228 (2014). https://doi.org/10.1039/C4SM01662A

[40] Saeva, F. D. & Wysocki, J. Induced circular dichroism in cholesteric liquid crystals. *J. Am. Chem. Soc.* **93**, 5928–5929 (1971). https://doi.org/10.1021/ja00751a075

[41] Slaney, A. J., Nishiyama, S. P., Styring, P. & Goodby, J. W. Twist inversion in a cholesteric material containing a single chiral centre. *J. Mater Chem*. **2**, 805–810 (1992). https://doi.org/10.1039/JM9920200805

[42] Dierking, I. *et al*. Investigations of the structure of a cholesteric phase with a temperature induced helix inversion and of the succeeding S_C* phase in thin liquid crystal cells. *Liq. Cryst.* **13**, 45–55 (1993). https://doi.org/10.1080/02678299308029052

[43] Hiller, S., Pikin, S. A., Haase, W., Goodby, J. W. & Nishiyama, I. Relaxation processes in the antiferroelectricphase as studied by dielectric spectroscopy. *Jpn. J. Appl. Phys*. **33**, L1170–L1173 (1994). https://doi.org/10.1143/JJAP.33

[44] Buivyads, M. *et al*. Collective and non-collective excitations in antiferroelectric and ferrielectric liquid crystals studied by dielectric relaxation spectroscopy and electro-optic measurements. *Liq. Cryst*. **23**, 723–739 (1997). https://doi.org/10.1080/026782997208000

[45] Huang, C.-C., Hsu, C.-C., Chen, L.-W. & Cheng, Y.-L. The effect of position of (S)-2-octyloxy tail on theformation of frustrated blue phase andantiferroelectric phase in Schiff base liquid crystals. *Soft Matter* **10**, 9343–9351 (2014). https://doi.org/10.1039/C4SM01829J

[46] Kirsch, P. Design and synthesis of nematic liquid crystals with negative dielectric anisotropy. *Liq. Cryst*. **26**, 449–452 (1999). https://doi.org/10.1080/026782999205236

[47] Kirsch, P., Reiffenrath, V. & Bremer, M. Nematic liquid crystals with negative dielectric anisotropy: Molecular design and synthesis. *Synlett* **4**, 389–396(1999). https://doi.org/10.1055/s-1999-2619

[48] Goodby, J. W., Patel, J. S. & Chin, E. Rotational damping and the spontaneous polarization in ferroelectric liquid crystals. *J. Phys. Chem.* **91**, 5151–5152 (1987). https://doi.org/10.1021/j100304a003

[49] Chandani, A. D. L. *et al*. Tristable switching in surface stabilized ferroelectric liquid crystals with a large spontaneous polarization. *Jpn. J. Appl. Phys.* **27**, L729–L732 (1988). https://doi.org/10.1143/JJAP.27.L729

[50] Yurtseven, H. & Kavruk, D. Analysis of the spontaneous polarization and the dielectric constant near the ferroelectric phase transition in TSCC. *Ferroelectrics* **367**, 190–200 (2008). https://doi.org/10.1080/00150190802375425

[51] Vaksman, V. M. & Panarin, Y. Measurement of ferroelectric liquid crystal parameters. *Mol. Mats.* **1**, 147–154 (1992). https://doi.org/10.21427/D7FF8R

[52] Hemine, J. *et al*. Dynamical properties of ferroelectricchiral liquid crystals by electro-optical and dielectric spectroscopy. *Spectrosc. Lett*. **41**, 285–291 (2008). https://doi.org/10.1080/00387010802286684

[53] Allagulov, A. I., Pikin, S. A. & Chigrinov, V. G. Bistable and monostable polarized states of a liquid-crystalline ferroelectric in an electric field. *Liq Cryst*. **5**, 1099–1105 (1989). https://doi.org/10.1080/02678298908026413

[54] Misra, A. K., Srivastava, A. K., Shukla, J. P. & Manohar, R. Dielectric and electro-optical parameters of two ferroelectric liquid crystals: A comparative study. *Phys. Scr*. **78**, 065602 (2008). https://doi.org/10.1088/0031-8949/78/06/065602

[55] Lyuu, J.-F., Chen, C.-C. & Lee, J.-Y. The anchoring energy coefficient of dye guest-host ferroelectric liquid crystals. *Mol. Cryst. Liq. Cryst*. **329**, 99–112 (1999). https://doi.org/10.1080/10587259908025930

[56] Manohar, R., Yadav, S. P., Pandey, K. K., Srivastava, A. K. & Misra, A. K. Comparative study of dielectric and electrooptical properties of pure and polymer ferroelectric liquid crystal composites. *J. Polym. Res*. **18**, 435–441 (2011). https://doi.org/10.1007/s10965-010-9434-0

[57] Seomun, S. S., Takanishi, Y., Ishikawa, K., Takezoe, H. & Fukuda, A. Evolution of switching characteristics from tristable to V-shaped in an apparently antiferroelectric liquid crystal. *Jpn. J. Appl. Phys*. **36**, 3586–3590 (1997). https://doi.org/10.1143/JJAP.36.3586

[58] Marino, L. *et al*. Dielectric characterization of an orthoconic antiferroelectric liquid crystal mixture. *Mol. Cryst. Liq. Cryst.* **558**, 120–126 (2012). https://doi.org/10.1080/15421406.2011.653717

[59] Nayek, P., Ghosh, S., Roy, S., Majumder, T. P. & Dabrowski, R. Electro-optic and dielectric investigations of a perfluorinated compound showing orthoconic antiferroelectric liquid crystal. *J. Mol. Liq.* **175**, 91–96 (2012). https://doi.org/10.1016/j.molliq.2012.08.020

[60] Ghosh, S., Nayek, P., Roy, S. Kr., Majumder, T. P. & Dabrowski, R. Dielectric relaxation spectroscopy and electro-optical studies of a new, partially fluorinated orthoconic antiferroelectric liquid crystal material exhibiting V-shaped switching. *Liq. Cryst*. **37**, 369–375 (2010). https://doi.org/10.1080/02678291003611367

[61] Havriliak, S. & Negami, S. A complex plane analysis of alpha-dispersions in some polymer systems. *J. Polym. Sci.* **14**, 99–117 (1966). https://doi.org/10.1002/polc.5070140111

[62] Panarian,Y. P., Kalinovskaya, O. & Vij, J. K. The investigation of the relaxation processes in antiferroelectric liquid crystals by broad band dielectric and electro-optic spectroscopy. *Liq. Cryst*. **25**, 241–252 (1998). https://doi.org/10.1080/026782998206399

[63] Pandey, M. B., Dhar, R. & Dąbrowski, R. Dielectric spectroscopy of a newly synthesized chlorinated analogue of MHPOBC antiferroelectric loquid crystals. *Ferroelectrics* **243**, 83–100 (2006). https://doi.org/10.1080/00150190600962119